Jurnal
Teknologi

Full Paper

PREDICTION OF FATIGUE IN RAIL PAD USING SIMULATION

Muhammad Faiz Anuar Amran, Abdul Malek Abdul Wahab*, Nor Fazli Adull Manan, Yupiter Hp Manurung

School of Mechanical Engineering, College of Engineering, Universiti Teknologi MARA, 40450, Shah Alam, Selangor, Malaysia

Article history
Received
12 June 2023
Received in revised form
30 July 2023
Accepted
20 August 2023
Published Online
20 December 2023

*Corresponding author
abdmalek@uitm.edu.my

Graphical abstract

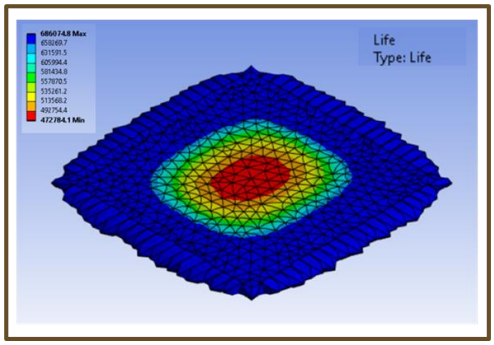

Abstract

The primary purpose of rail pads is to prevent cracking in concrete connections, which is assumed to be caused by the passing train's impact and vibration generated by movement from its wheels. To ensure the usage of rail pads is reliable and safe, failure and fatigue life prediction need to be done. However, analyzing fatigue conditions using the experimental method is time-consuming and costly. Thus, this work aims to develop a finite element model for analyzing the fatigue and life cycle of the rail pads. By using the simulation method, the time and cost of analyzing the process can be reduced. The rail fastening system model comprises a steel rail, rail pad, and concrete sleeper. The Mooney-Rivlin model was used to develop the rail pad, and the isotropic elasticity model was used for the steel rail and concrete sleeper. Using the modified Goodman theory, this study was able to estimate the fatigue life of the rail pad in terms of the number of cycles for a range of compressive forces and toe load. The findings show that a toe load at 18 kN shows more life cycle compared to a higher toe load of 35 kN with more than 50% difference. The life cycle also reduces as the load applies increases. This concludes that the fatigue life of the rail pad is greatly dependent on the toe load condition and compressive load. The rail pad is less durable under greater compressive load circumstances.

Keywords: Rail Pad, Finite Element Method, Fatigue, Hyper elastic, Toe Load

Abstrak

Tujuan utama pad rel adalah untuk mengelakkan keretakan pada sambungan konkrit, yang diandaikan berpunca daripada hentaman dan getaran kereta api yang lalu yang dihasilkan oleh pergerakan dari rodanya. Untuk memastikan penggunaan pad rel boleh dipercayai dan selamat, ramalan hayat kegagalan dan keletihan perlu dilakukan. Walau bagaimanapun, menganalisis keadaan keletihan menggunakan kaedah eksperimen memakan masa dan kos yang tinggi. Oleh itu, kerja ini bertujuan untuk membangunkan model elemen terhingga untuk menganalisis keletihan dan kitaran hayat pad rel. Dengan menggunakan kaedah simulasi, masa dan kos menganalisis proses dapat dikurangkan. Model sistem pengikat rel terdiri daripada rel keluli, pad rel dan tempat tidur konkrit. Model Mooney-Rivlin digunakan untuk membangunkan pad rel, dan model keanjalan isotropik digunakan untuk rel keluli dan ranjang landas. Dengan menggunakan teori Goodman yang diubah suai, kajian ini dapat menganggarkan jangka hayat pad rel dari segi bilangan kitaran untuk julat daya mampatan dan beban kaki. Dapatan menunjukkan bahawa beban kaki pada 18 kN menunjukkan lebih banyak kitaran hayat berbanding

dengan beban kaki lebih tinggi iaitu 35 kN dengan perbezaan lebih daripada 50%. Kitaran hayat juga berkurangan apabila beban dikenakan meningkat. Ini menyimpulkan bahawa hayat keletihan pad rel sangat bergantung kepada keadaan beban kaki dan beban mampatan. Pad rel kurang tahan lama di bawah keadaan beban mampatan yang lebih besar.

Kata kunci: Pad Rel; Kaedah Elemen Terhingga; Keletihan; Hiperelastik; Beban Kaki

1.0 INTRODUCTION

A rail system's long-term viability and safety heavily depend on the condition of its infrastructure, which is expensive to maintain. In addition to the social and economic ramifications, any inconvenience to the railway service must be minimal. Although crucial, track performance and maintenance management could be better understood and forecasted from a scientific perspective. Among the essential aspects of rail track performance is ensuring that operational breakdowns are avoided at all costs. Therefore, fatigue analysis and strength evaluation are fundamental in the design procedure to ensure the safety and reliability of the mechanical rubber components of the rail track [1]. The lack of these analyses and evaluations leads to an increase in the gauge-expanding accident rate and the cost of running the train due to the increased amount of electricity required to run it [2].

The dynamic and static preloading of the rails is performed using different approaches by the rail fastening system and the wheel load of trains. When this wheel load moves along a path, it causes local deformation and puts preload on the track components [3]. As an extra safety measure, the design of each part of the overall fastening system must be solid and safe so that the vehicles can operate without any problems [4].

The attaching mechanism for rails was crucial, allowing them to function as designed [5]. The rail pad was a vital component of the fastening mechanism [6], [7], [8]. The rail pads, mounted on rail seats, are designed to relieve the dynamic stress brought on by axle loads and wheel contact during conventional and irregular train travel [9], [5]. A rail pad can provide additional protection for ballast when dealing with more significant dynamic overloads [5], [10], [11]. The rail pad provided most of the route's required vertical stiffness, allowing for the successful operation of both the ballasted track and the slab track [12], [13].

The hyperelastic materials used to make the rail pads have significant nonlinear and energy dissipation mechanical characteristics, which are strongly affected by the loads and environmental parameters [14]. When exposed to external forces, hyperelastic structures often undergo significant strains.

The analysis of the rail pad condition using numerical methods has attracted the attention of many researchers. To investigate the impact of the rail pad's nonlinearity and preload on track vibration under static and dynamic loads, Koroma *et al*. simulated the rail pad using Finite Element (FE) analysis [15]. Their results suggested that these elements do influence the track's vibration. Rail pads, clips, and ballast were employed in Oregui *et al*.'s simulation of railway tracks using linear spring/dashpot components [31]. The study examined the effects of preload and stiffness characteristics on the dynamic stiffness of the track. Zhang *et al*. modeled the fastening system using finite element (FE) to study the effect of preload on fastening system performance. The vibration of the railway bridge was altered by the fastening system's nonlinear state, as reported by Yang *et al*. [16]. Using FE, Liu *et al*. investigated how nonlinearity affected the mechanical properties of the fastening system [17]. Othman *et al*. characterized the static stiffness of different materials of rail pad ethylene propylene diene monomer (EPDM), thermoplastic elastomers (TPEs), and ethylene vinyl acetate (EVA). Each of these materials shows different conditions of static stiffness under the effect of temperature and toe load [18].

However, the prediction of fatigue life on rail pads using numerical methods has not been well studied. Failure analysis and fatigue life prediction must be performed on hyperelastic materials during the design phase to ensure their long-term durability and safety [19].

Therefore, this study aimed to use numerical computation to predict the TPE rail pad's fatigue life. The rail pad's fatigue life was evaluated under several conditions of applied load and toe load. The fastening mechanism was modeled in three dimensions (3D) using finite element (FE) software.

2.0 METHODOLOGY

CATIA V5 was implemented to construct geometric models for the steel rail, rail pad, and concrete sleeper. The item's dimensions were established using the existing design following previous literature research [18]. Figure 1 shows the isometric geometry of a steel rail, rail pad, and concrete sleeper. Figure 2

shows the rail pad's isometric design. Table 1 has the exact dimensions of all three geometry.

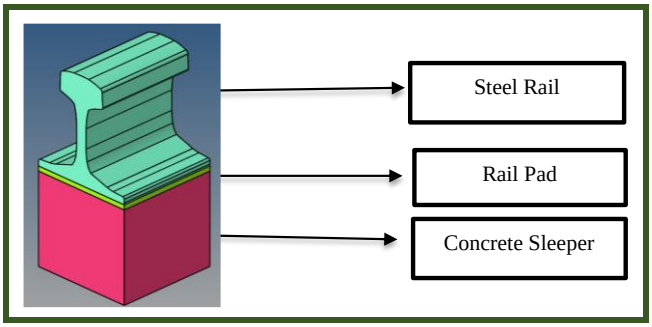

Figure 1 Isometric View of the Steel Rail, Rail Pad and Concrete Sleeper

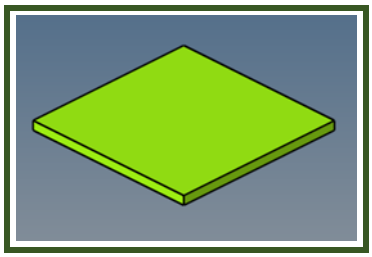

Figure 2 Isometric View of the Rail Pad

Table 1 Rail Pad Dimensions

Parameter	Specifications (mm)
Length	150
Height	8
Width	150

Theoretical and Mathematical Modeling Elastic Deformation

To verify that the geometry of the rail steel, rail pad, and concrete sleeper was designed accurately, FEM was employed to compute the elastic deformation of the rail pad. The outcome of the elastic deformation was compared with experimental data from the previous research article for validation analysis. A formula for determining the Elastic deformation (δ) is as follows.

$$\delta = \frac{\sigma \times L}{E} = \frac{F \times L}{A \times E} \quad (1)$$

where δ represents the Normal stress, E is the elasticity modulus, F is the force, L is the length, and A the area. The formulas for determining the elasticity modulus (E) is as follows;

$$E = \frac{\sigma}{\varepsilon} \quad (2)$$

Hence, σ the normal stress and the strain. Normal stress σ may be determined using:

$$\sigma = \frac{P}{A} \quad (3)$$

Fatigue Life Prediction

Elastomers material displays complex mechanical behavior that exceeds the linear elastic model, involving massive elastic deformation, plastic, and viscoelastic characteristics, and stress softening. As empirical forecasts of fatigue life for elastomers, maximum principal strain, maximum principal stress, and strain energy density have been used. In this study, the Modified Goodman technique was used to calculate the fatigue life of this hyperelastic rail pad material. The Modified Goodman is identical to the Linear mean stress correction since the decrease of the allowable limits stress range is linear. The Modified equation is given as follows:

$$\frac{\sigma_a}{\sigma_N} + \frac{\sigma_m}{\sigma_{UTS}} = 1 \quad (4)$$

Where represents the amplitude of the applied cyclic stress, the mean of the applied stress, σ_N the fully reversed bending fatigue strength at a given number of cycles, and the ultimate tensile strength.

The fatigue strength σ_m is isolated:

$$\sigma_a = \sigma_N \left(1 - \frac{\sigma_m}{\sigma_{UTS}}\right) \quad (5)$$

Parameter Identification

Elements of track constructions' stiffness and attenuation were examined in the simulation test shown in Table 2 [18]. The outcomes of the simulation tests may be affected by adjusting the parameters.

Table 2 Basic Properties of Rail Pad, Steel Rail, and Concrete Sleeper Structures [18]

Types of track structures	Parameter	Designation	Value	Unit
TPE (rail pad)	Density	ρ_T	1300	kg m-3
	Coefficient of Thermal Expansion	α_T	0.00013	C-1
	Young's Modulus	E_T	30	MPa
	Poisson's Ratio	υ_T	0.41	
	Tensile Yield Strength	σ_T	34.5	MPa

Types of track structures	Parameter	Designation	Value	Unit
	Tensile Ultimate Strength	σ_{uT}	52	MPa
	Initial Shear Modulus Mu	G	10638000	Pa
	Incompressibility Parameter D1	K	3.6E-08	Pa-1
Structural Steel (rail)	Density	ρ_S	7850	kg m-3
	Coefficient of Thermal Expansion	α_S	0.000012	C-1
	Young's Modulus	E_S	200000	MPa
	Poisson's Ratio	υ_S	0.3	
	Tensile Yield Strength	σ_S	250	MPa
	Compressive Yield Strength	σ_{cS}	250	MPa
	Tensile Ultimate Strength	σ_{uS}	460	MPa
	Compressive Ultimate Strength	σ_{cuS}	0	MPa
Concrete (Sleeper)	Density	ρ_C	2300	kg m-3
	Coefficient of Thermal Expansion	α_C	0.000014	C-1
	Young's Modulus	E_C	30000	MPa
	Poisson's Ratio	υ_C	0.18	
	Tensile Yield Strength	σ_C	0	MPa
	Compressive Yield Strength	σ_{cC}	0	MPa
	Tensile Ultimate Strength	σ_{uC}	5	MPa
	Compressive Ultimate Strength	σ_{cuC}	41	MPa

Simulation Test Campaign

ANSYS was implemented to describe the elastic deformation test and fatigue life simulation of the rail pad model. The most common hyperelastic material, Thermoplastic Elastomer (TPE), was under the effects of the varied loading configuration, toe load, and constant amplitude loading.

The simulation was tested while subjected to the varying forces generated by the train's wheels. All of the applied load and toe load parameters must be strictly adhered to acquire the correct result of the elastic deformation using the experimental data in the prior study [20]. These variables and the toe load were used to create the simulation test campaign of elastic deformation and fatigue life prediction.

Boundary Conditions and Load

Boundary conditions are established on the investigated physical domain and must be defined iteratively throughout this FEM simulation. The boundary condition approach was developed to identify conditions under which the solution would converge to a fair value. In the finite element methods, symmetric boundary conditions are restrictions that can lessen the load on the computer's resources and expedite simulations.

The contact location between a particular part was determined to ensure that the simulation calculations were carried out correctly. The default friction coefficient of 0.14 was applied to the friction forces between the rail and the rail pad and the rail pad and the concrete sleeper. By applying the frictionless support to the selected surface, the contact surface can carry out the shear forces, preventing the assembly geometries from sliding with each other at applying and roe load during the simulation. In scientific circles, this was called "sticking." As seen in Figure 3, the concrete sleeper underneath was reinforced with a permanent fixture. As can be seen in Figure 4, frictionless support was employed on both the rail pad's four sides and the rail's two sides.

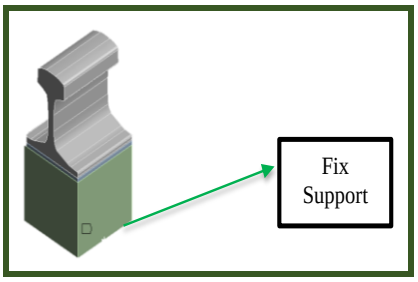

Figure 3 Fixed Support Applied on the Bottom Surface of the Concrete Sleeper

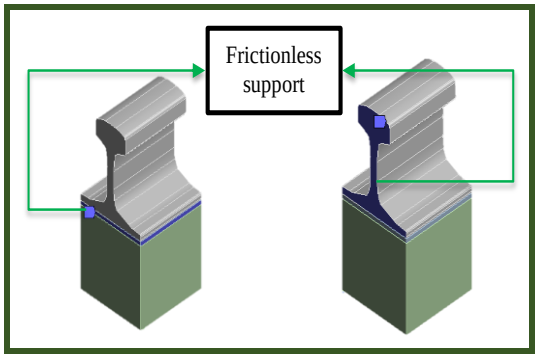

Figure 4 Frictionless Support on the Sides of Rail Pad and Rail

The applied load and toe load were considered in this simulation. The following nine loads (10kN, 20kN, 30kN, 50kN, 60kN, 70kN, 80kN, and 90kN) were used in the simulation.

The toe load was typically set at 18kN. Nevertheless, it was typical if the toe load was too loose or tight. Four different conditions of the load. First, 18kN represents the correct assembly of the system in this circumstance. After then, the fastening system failed under an extreme case of 1kN. Finally, we looked at two further criteria depending on whether the fastener might be under-torqued, at 9kN, or over-torqued, at 25kN. Figure 5 shows the applied load and toe load in the simulation.

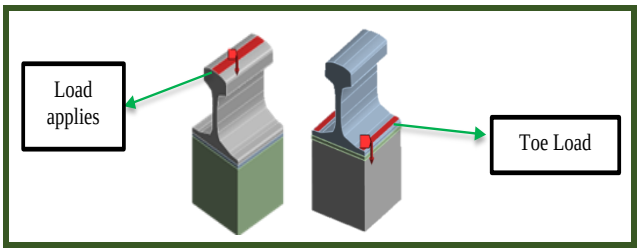

Figure 5 Load Applies to the Model

Mesh Type

The tetrahedron meshing type was used for the simulation's meshing setting for the rail's structure. A tetrahedral mesh is like a 2D triangular mesh but in 3D. Most of the time, the tetrahedral mesh is built as equilateral tetrahedra, like in systems with a circular curve. However, this type of mesh is also built as isosceles tetrahedra when a system is not symmetrical. Compared with other types of mesh, the tetrahedral mesh can be flexible and easily fit into any geometry, and it would be much more accurate than a simple cube grid in 3D or a square grid in 2D [21]. Due to the complex shape model for the rail structure, a 3D tetrahedral mesh was introduced, as shown in Figure 6.

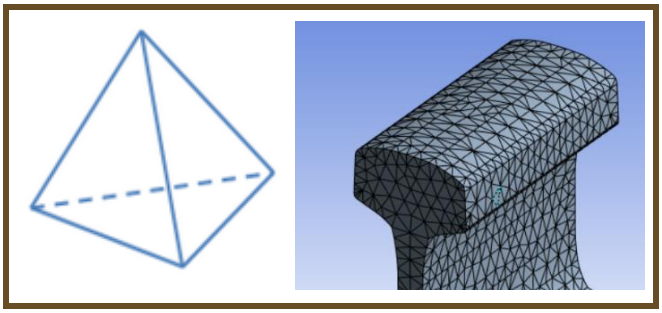

Figure 6 Tetrahedral Meshing Type

Rail Pad

The rail pad was modeled using solid elements, and the cross-sectional shape was assumed to be nominal. To develop the rail pad material, the thermoplastic elastomers (TPE) material, which has characteristics of rubber material, was used. A hyper-elastic substance that exhibited a nonlinear behavior had characteristics of rubberized material. The Mooney-Rivlin model was used to analyze the elastomer's behavior. Mooney Rivlin was an expanded model of the neo-Hookean model, which incorporates formulation and model to describe the hyper-elastic behavior of the material [22]. For this study, the Mooney-Rivlin model is considered the second invariant component. Mooney [23], developed the strain energy density as a two-parameter model in its most fundamental version, which is stated as follows:

$$W_M = C_1(\overline{I_1} - 3) + C_2(\overline{I_2} - 3) + D_1(J-3)^2, \quad (6)$$

Where W_M represents the strain energy density of the two-parameter Mooney model, then the and represents the coefficients. Hence, by applying;

$$\lambda_2 = \lambda_3 = \lambda_1^{-v}, \quad (7)$$

the axial stress can be obtained from the two-parameter Mooney-Rivlin model formula as:

$$\sigma_{uni} = \frac{4(1+v)}{3}\lambda_1^{-\frac{5+2v}{3}}\left(\lambda_1^{2+2v} - 1\right)\left(C_1 + C_2\lambda_1^{-\frac{2v(1+v)}{3}}\right) + 2D_1(1-2_v)\lambda_1^{-2v}(J-1) \quad (8)$$

By considering that the structure was incompressible, Eq. (8) becomes:

$$\sigma_{uni} = 2C_1(\lambda - \lambda^{-2}) + 2C_2(1 - \lambda^{-3}) \quad (9)$$

Steel Rail and Concrete Sleeper

The steel rail and the concrete sleeper design use a solid element with nominal cross-sectional geometry. Due to the nature of the applied loads, which are insufficient for plastic deformation of the steel rail, the rails as elastic. The material properties of the steel rail and concrete sleepers contrast with the behavior of railway passages, which often cause plastic deformation of the rail near-failures. Because the linear elastic material properties for non-cracked concrete sleepers can be defined as under railways passages, Gustavson and Gylltoft reasoned that[24], despite the sleepers being constructed of reinforced concrete, elastic material was used. Traditionally, linear elasticity was used to define the minor strain mechanical behavior of solid materials like concrete and steel. In addition, the theory of elasticity can be expressed as isotropic elasticity in its most straightforward form. This idea's stress was proportional to pressure and independent of material body orientation.

Validation of Simulation

To perform simulation analysis, the finalized design of the rail geometry was transferred into ANSYS software. The experimental data from previous research has been set as a validation reference. Similar boundary conditions and loads were applied in the simulation. The percentage error of rail pad deformation was computed as a comparison between the current simulation and previous experimental work [34].

In addition, the mesh convergence test was conducted to ensure the accuracy of the simulation results [25]. Inaccurate simulation result often occurs if the mesh becomes too coarse. However, as the mesh gets more detailed in sizing, it also requires more time to run the simulation.

3.0 RESULTS AND DISCUSSION

Mesh Convergences

Table 3 shows the mesh setting considered for deformation at 60 kN. Results show that the FEM with a more significant number of elements requires more time to complete the simulation. According to the table, the rail pad model with a meshing size of 7 mm and 6.5 mm produced the nearest reading of deformation compared to the reference work [20] with the number of elements 24652 and 26002 respectively. However, for the number of elements 26002, the time for the simulation is higher. Therefore, a meshing size of 7 mm is used in this work.

Table 3 Mesh Setup Parameters

Element Size (mm)	Number of Element	Time Consumption (minute)	Total deformation at 60kN (mm)
6.5	26002	32	0.5299
7	24652	20	0.5229
7.5	23252	15	0.5413
8	22054	13	0.4949
8.5	21307	12	0.4674
9	20941	7	0.4597
9.5	20583	5	0.4225

Validation of Simulation

The validation was performed with experimental data from a previous research paper. Figure 7 shows that the simulation data were in agreement with experimental data from Sainz-Aja *et al*. [20].

Table 4 compares the simulation and experimental data's deformation results. The Simulation model accuracy must expect a 10 percent error rate or below. However, the data indicate several percentage errors that exceed 10 percent of error, mostly at applied load conditions at 10kN and 20kN for each condition. The significant percentage error of deformation caused by various missteps while completing the finite element method, including modeling the hyperelastic, meshing size, boundary conditions, and surface contacts, and specifying the geometry's mesh quality.

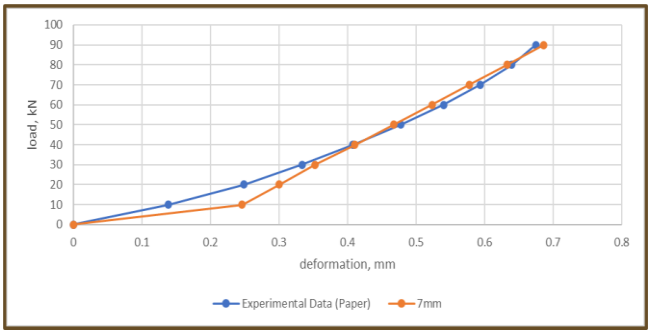

Figure 7 Comparison of Simulation Results and Experimental Results

Table 4 Error Percentage for Simulation and Experimental Data with 7mm

No.	Load (kN)	Deformation (mm)		Percentage Error (%) (7mm mesh size)
		Ref [20]	Simulation (7mm mesh size)	
1	0	0	0	0
2	10	0.1382	0.2464	78.292
3	20	0.2488	0.3003	20.699
4	30	0.3335	0.3529	5.817
5	40	0.4072	0.4107	0.860
6	50	0.4773	0.4673	2.095
7	60	0.5399	0.5229	3.149
8	70	0.5934	0.5779	2.612
9	80	0.6394	0.6323	1.110
10	90	0.6744	0.6863	1.765

Fatigue Life Prediction

Figure 8 shows the contour diagram for the fatigue life simulation of the rail pad. The rail pad will fail due to yield point stresses when repeatedly subjected to repeating stresses. The constant amplitude loading type utilized in this fatigue simulation was zero-based. Hence the stress cycle was repeated with the scale factor set to 2. This simulation implements the stress life technique, which uses the S-N curve of the TPE rail pad model to compute the rail pad's life cycle under varying loading and toe load influence. The S-N curve for this TPE rail pad was used as a reference in the earlier study article to approximate the life cycle[26]. According to Figure 8, the red area implies a minimum number of life cycles of 472784.1 cycles. Meanwhile, the blue region represents the maximum number of life cycles (686074.8). As a result, the rail

pad will fail at 472784.1 cycles in applying loading at 90kN.

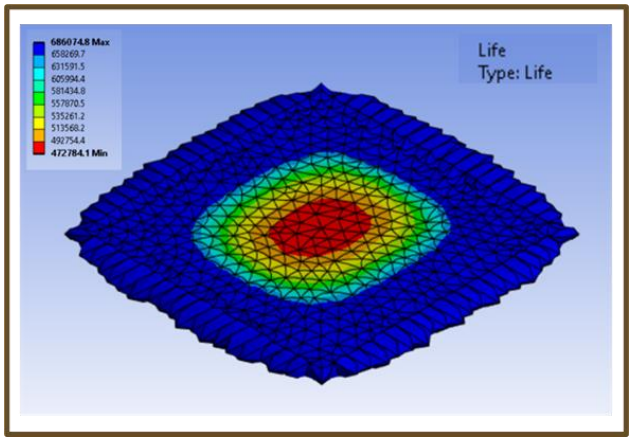

Figure 8 Fatigue Life Simulation of Rail Pad

The fatigue life analysis is a method used to determine the number of cycles the rail pad material can withstand before failure occurs. Besides, to predict the fatigue life of the rail pad subjected to varying quantities of cyclic loading, the outcome of the simulation was used to construct Figure 9, which has a graph that illustrates the load-life cycle.

The simulation results show that the number of cycles a material can withstand decreases as the applied load increases. In this case, when the load was applied at 130 kN or above, the number of life cycles for the rail pad was 0, indicating that the TPE rail pad would fracture immediately at this load level. When the load was decreased to 90 kN, the number of cycles increased to 472784.10. Furthermore, when the load was further decreased to 60 kN, the number of cycles increased even more to 686074.80. The fundamental concept of fatigue is that the greater the stress reduction, the greater the number of cycles a material can endure before fracture. The result observation is consistent with that. Therefore, it can be concluded that the simulation result was consistent with the fundamental concept of fatigue, which holds that the greater the magnitude of the stress, the fewer cycles a geometry can endure before the fracture.

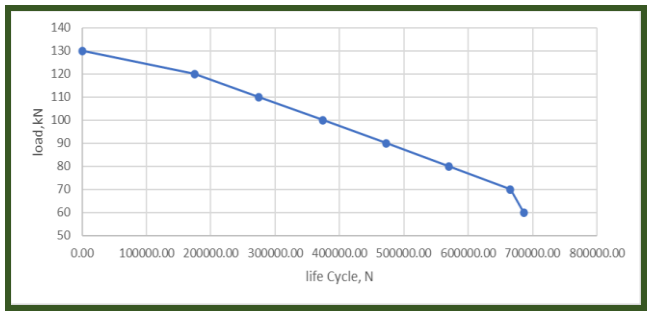

Figure 9 Life Cycle of Rail Pad Under Various Applied Load

The fatigue life analysis of the rail pad under three distinct toe load circumstances reveals that as the toe load rises, the number of cycles before failure decreases as shown in Figure 10. The rail pad's life cycle turned zero at a comparable amount of applied load, which is 130 kN, for toe loads of 18 kN and 25 kN. At these toe load levels, the rail pad would fail quickly. At an applied load of 120 kN, the number of cycles of the rail pad decreased to zero at 35 kN toe load. The results demonstrate that the rail pad with a toe load of 35kN is less robust to greater toe loads and fails at a lower applied force. The findings show that the fatigue life of the rail pad is greatly dependent on the toe load condition and that the rail pad is less durable under greater toe load circumstances.

Furthermore, the fatigue life study findings suggest that when the toe load is 18 kN, the rail pad has the best fatigue life cycle. Even with greater applied loads, the rail pad has a rather large number of cycles before failure in this circumstance. When the applied load is 70 kN, for example, the rail pad has a cycle count of 665320.10, which is much larger than the number of cycles at the same applied load for the other two situations, 25 kN and 35 kN. The number of cycles at 70 kN applied load was 607550 at 25 kN, while the number of cycles at 120 kN is zero at 35 kN. Therefore, the rail pad is more robust under the 18 kN toe load condition than under the other two circumstances. As a result, the ideal state for the rail pad in terms of the fatigue life cycle is when the toe load is 18 kN.

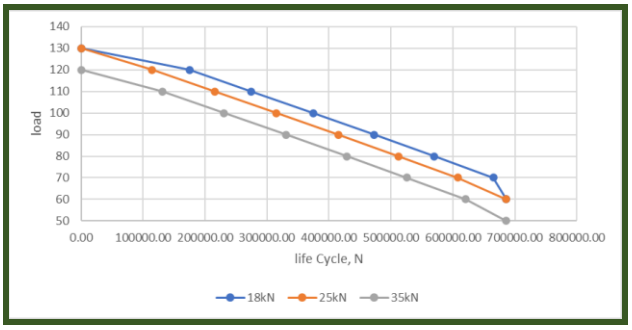

Figure 10 Comparison of Rail Pad Life Cycle under Three Toe Load Conditions

Damage Accumulation

A fatigue life study was conducted on a TPE rail pad to determine its durability over a specific design life. The study used ANSYS software and applied load and toe load conditions of 90 kN and 18 kN, respectively, with a maximum number of cycles of 472,784. The study produced an accumulative damage curve, which plots the cumulative damage against the design life as shown in Figure 11. The curve indicates that damage to the component increases with increasing design life, and it will fail when the damage reaches 1.0, which is the point at

which it has reached the end of its designed service life. The maximum life cycle of the component is 472,784 cycles, showing that it has a margin of safety.

The cumulative damage curve can be used to estimate the remaining life of a component and improve its design. The remaining life of the component may be estimated by determining the number of cycles necessary to sustain the remaining percentage of the damage, and the curve can be used to establish the component's maximum permissible load or the number of cycles it can endure before failing. In summary, an accumulative damage curve is a crucial tool in evaluating the fatigue life of components and designing them for optimal durability.

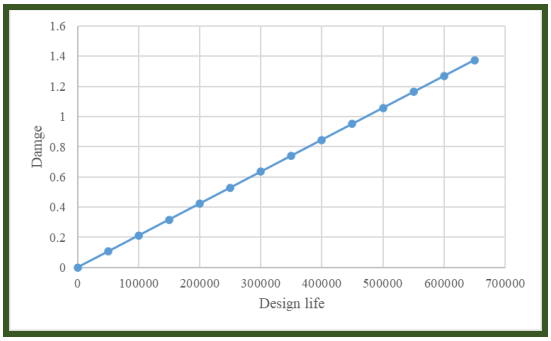

Figure 11 Damage Accumulation Curve

4.0 CONCLUSION

In conclusion, the fatigue life of a TPE rail pad model was predicted using the finite element approach that is offered in the ANSYS software. According to the study's findings, the TPE rail pad model exhibited a high quality of fatigue resistance and could maintain its stability for many cycles despite being subjected to various applied and toe load circumstances. The ANSYS software enabled a comprehensive and exact study of the TPE rail pad model, generating significant insights into its performance under various loading circumstances. Using the S-N curve of the TPE rail pad model, the simulation was able to accurately estimate the life cycle of the rail pad under a variety of loading parameters and the impact of the toe load.

The simulation findings may be used to identify the optimized design of the TPE rail pad, which can resist the stresses of its intended usage while also ensuring that it is safe and reliable while it is being used. In addition, the simulation may serve as a point of reference for the validation test performed on the rail pad model. The simulation may be used to estimate the most probable areas of failure on the rail pad and assist in identifying the crucial spots of the rail pad.

Several recommendations could well be made to enhance the finite element approach of predicting rail pad fatigue life. To begin, verify that the boundary conditions and loads employed in the simulation are as exact as possible, since they have a substantial influence on the findings. This may be accomplished by carrying out tests and measurements to identify the actual loading and boundary conditions that the rail pad will face in its intended application. Second, it is critical to select the most exact TPE rail pad material parameters available to guarantee that the simulation results are as accurate as possible. It is possible to do this by performing material tests such as tensile, compression, and fatigue tests. Finally, mesh convergence must be explored. The reliability of the findings is impacted by the complexity of the simulation. The simulation results may be improved by using a finer mesh size. It is crucial, however, to discover the optimum element size that exchanges accuracy for processing resources needed to execute the simulation.

Conflicts of Interest

The author(s) declare(s) that there is no conflict of interest regarding the publication of this paper.

Acknowledgment

The authors gratefully acknowledge the College of Engineering, Universiti Teknologi MARA for the preparation, execution, writing, and publication of this article.

References

[1] B. Suryatal, H. Phakatkar, K. Rajkumar, and P. Thavamani. 2015. Fatigue Life Estimation of an Elastomeric Pad by ε-N Curve and FEA. *J. Surf. Eng. Mater. Adv. Technol.* 5(2): 85-92. Doi: 10.4236/jsemat.2015.52010.

[2] D. Sung and S. Hong. 2020. A Simple Method to Assess Replacement Period of Polyurethane Railpad in Urban Railway. *Constr. Build. Mater.* 248: 118607. Doi: 10.1016/j.conbuildmat.2020.118607.

[3] S. Kaewunruen and A. M. Remennikov. 2008. An Alternative Rail Pad Tester for Measuring Dynamic Properties of Rail Pads Under Large Preloads. *Experimental Mechanics*. 48: 55-64. Doi: 10.1007/s11340-007-9059-3.

[4] A. Kalliainen, P. Kolisoja, and A. Nurmikolu. 2016. 3D Finite Element Model as a Tool for Analyzing the Structural Behavior of a Railway Track. *Procedia Eng.* 143: 820-827. Doi: 10.1016/j.proeng.2016.06.133.

[5] C. Ngamkhanong, Q. Y. Ming, T. Li, and S. Kaewunruen. 2020. Dynamic Train-track Interactions Over Railway Track Stiffness Transition Zones using Baseplate Fastening Systems. *Eng. Fail. Anal.* 118(May): 104866. Doi: 10.1016/j.engfailanal.2020.104866.

[6] X. Ge, L. Ling, X. Yuan, and K. Wang. 2020. Effect of Distributed Support of Rail Pad on Vertical Vehicle-track Interactions. *Constr. Build. Mater.* 262: 120607. Doi: 10.1016/j.conbuildmat.2020.120607.

[7] D. Ferreño *et al.* 2021. Prediction of Mechanical Properties of Rail Pads under In-service Conditions through Machine Learning Algorithms. *Adv. Eng. Softw.* 151(July 2020). Doi:

10.1016/j.advengsoft.2020.102927.
[8] Z. Zhang, B. Andrawes, and R. E. J. 2015. Parametric Study on the Distribution of Longitudinal Load in Railway Track under Dynamic Wheel Loading Using Finite Element Analysis. *Int. J. Civ. Eng.* 2(5): 13-27. Doi: 10.14445/23488352/ijce-v2i5p106.
[9] J. Pombo and J. Ambrósio. 2012. An Alternative Method to Include Track Irregularities in Railway Vehicle Dynamic Analyses. *Nonlinear Dyn.* 68(1-2): 161-176. Doi: 10.1007/s11071-011-0212-2.
[10] M. Sol-Sánchez, F. Moreno-Navarro, and M. C. Rubio-Gámez. 2014. The Use of Deconstructed Tire Rail Pads in Railroad Tracks: Impact of Pad Thickness. *Mater. Des.* 58: 198-203. Doi: 10.1016/j.matdes.2014.01.062.
[11] J. Chen and Y. Zhou. 2020. Dynamic Vertical Displacement for Ballastless Track-subgrade System under High-speed Train Moving Loads. *Soil Dyn. Earthq. Eng.* 129(November 2019): 105911. Doi: 10.1016/j.soildyn.2019.105911.
[12] K. Wei, F. Wang, P. Wang, Z. X. Liu, and P. Zhang. 2017. Effect of Temperature- and Frequency-dependent Dynamic Properties of Rail Pads on High-speed Vehicle–track Coupled Vibrations. *Veh. Syst. Dyn.* 55(3): 351-370. Doi: 10.1080/00423114.2016.1267371.
[13] E. Koch, P. Hudacsek, R. Szepesházi, and O. Kegyes-Brassai. 2018. 3D Modelling of Train-track Interaction at Bridge Transition. *Ce/Papers*. 2(2-3): 695-700. Doi: 10.1002/cepa.751.
[14] B. Yenigun, E. Gkouti, A. Czekanski, G. Barbaraci, and K. P. Jankowski. 2020. Comparison of Elasto-Mechanical Behavior of Rubbers. *Conference: Canadian Society for Mechanical Engineering International Congress.*
[15] S. G. Koroma, M. F. M. Hussein, and J. S. Owen. 2015. Influence of Preload and Nonlinearity of Railpads on Vibration of Railway Tracks under Stationary and Moving Harmonic Loads. *J. Low Freq. Noise Vib. Act. Control*. 34(3): 289-306. Doi: 10.1260/0263-0923.34.3.289.
[16] S. C. Yang, H. H. Kim, and J. S. Kong. 2017. Evaluation of Uplift Forces Acting on Fastening Systems at the Bridge Deck End Considering Nonlinear Behaviors of the Fastening Systems. *J. Korean Soc. Railw.* 20(4): 521-528. Doi: 10.7782/JKSR.2017.20.4.521.
[17] Y. Liu, H. P. Yin, Y. Luo, and J. Zhang. 2018. Finite Element Analysis and Experimental Investigation of Nonlinear Features of Rail Fastening Systems. *Proc. Inst. Mech. Eng. Part F J. Rail Rapid Transit*. 232(3): 873-894. Doi: 10.1177/0954409717701779.
[18] M. I. H. Othman, A. M. A. Wahab, M. S. Hadi, and N. M. Noor. 2022. Assessing the Nonlinear Static Stiffness of Rail Pad using Finite Element Method. *J. Vibroengineering*. 24(5): 921-935. Doi: 10.21595/jve.2022.22293.
[19] A. Ali, M. Hosseini, and B. B. Sahari. 2009. Fatigue Life Modeling For Elastomeric Materials: A Review. *Int. Rev. Mech. Eng.* 3(3): 332–338. Doi: 10.15866/ireamt.v2i1.1143.
[20] J. A. Sainz-Aja, I. A. Carrascal, D. Ferreño, J. Pombo, J. A. Casado, and S. Diego. 2020. Influence of the Operational Conditions on Static and Dynamic Stiffness of Rail Pads. *Mech. Mater.* 148(June). Doi: 10.1016/j.mechmat.2020.103505.
[21] B. M. Klingner and J. R. Shewchuk. 2008. Aggressive tetrahedral Mesh Improvement. *Proc. 16th Int. Meshing Roundtable, IMR 2007*. 3-23. Doi: 10.1007/978-3-540-75103-8_1.
[22] B. Kim *et al.* 2012. A Comparison among Neo-Hookean Model, Mooney-Rivlin Model, and Ogden Model for Chloroprene Rubber. *Int. J. Precis. Eng. Manuf.* 13(5): 759-764. Doi: 10.1007/s12541-012-0099-y.
[23] H. B. Khaniki, M. H. Ghayesh, R. Chin, and M. Amabili. 2022. A Review on the Nonlinear Dynamics of Hyperelastic Structures. *Nonlinear Dyn.* 110: 963-994. Doi: 10.1007/s11071-022-07700-3.
[24] E. Kabo, J. C. O. Nielsen, and A. Ekberg. 2006. Prediction of Dynamic Train-track Interaction and Subsequent Material Deterioration in the Presence of Insulated Rail Joints. *Veh. Syst. Dyn.* 44(SUPPL. 1): 718-729. Doi: 10.1080/00423110600885715.
[25] H. Patil and P. V. Jeyakarthikeyan. 2018. Mesh Convergence Study and Estimation of Discretization Error of Hub in Clutch Disc with Integration of ANSYS. *IOP Conf. Ser. Mater. Sci. Eng.* 402(1). Doi: 10.1088/1757-899X/402/1/012065.
[26] L. Chen, C. Yang, H. Wang, D. T. Branson, J. S. Dai, and R. Kang. 2018. Design and Modeling of a Soft Robotic Surface with Hyperelastic Material. *Mech. Mach. Theory*. 130: 109-122. Doi: 10.1016/j.mechmachtheory.2018.08.010.